Microelectrode Array for Chronic Deep-Brain Microstimulation and Recording

Douglas McCreery, Albert Lossinsky, Victor Pikov, and Xindong Liu

***Abstract*—We have developed an array of microelectrodes that is suitable for long-term implantation into the subthalamic nucleus (STN) or the globus pallidus and is able to record from single neurons, as well as deliver localized microstimulation. This device can be used to investigate the mechanisms by which deep brain stimulation can ameliorate the symptoms of Parkinson's disease and other movement disorders, and also may be the basis for a new clinical tool for the treatment of Parkinson's disease, by capitalizing on the high spatial specificity of intranuclear microstimulation. The array includes 16 activated iridium microelectrodes, 5–6 mm in length, within a cluster approximately 1.8 mm in diameter. We have fabricated the array using materials carrying the USP Category VI classification, and we have developed an apparatus and a procedure for implanting the microelectrode arrays into the deep brain.**

Ten arrays have been implanted into the STN of domestic cats, and one into the internal segment of the globus pallidus, for 140–415 days. During that time, we were able to record action potentials from individual neurons, on 4 to 8 of the 16 channels. The microelectrode' active surface areas ranged from 500 to 2 000 μm^2. Controlled-current pulses, 26.5 μA in amplitude and 150 μs/phase in duration (4 nC/phase) were used to excite neurons in the cat's STN. In addition to direct activation, the stimulus modulated the neuronal activity over a distance of at least 1.2 mm from the site of stimulation. These parameters did not induce histologically detectable changes around the tip sites after 35 hours of stimulation at 100 Hz (7 hours of stimulation per day, on 5 successive days), if the electrode' active surface area was 1 000 μm^2 or greater.

***Index Terms*—Cats, chronic implant, deep brain stimulation, microstimulation, safety of electrical stimulation, subthalamic nucleus.**

I. Introduction

ELECTRICAL stimulation in deep brain structures [deep brain stimulation (DBS)] has developed into an effective treatment modality for advanced Parkinson's disease and essential tremor. DBS also is being evaluated as a treatment for other neurological conditions and appears to be helpful in the treatment of several types of dystonia and hyperkinetic disorders. (For recent reviews of these topics, see [1]–[5]. While the range of clinical applications for DBS has expanded in recent years, its mechanism of action remains unclear (e.g., [4] and [6]). Studies directed toward an elucidation of the physiologic underpinnings of DBS certainly would be aided by a microelectrode array that could be implanted chronically into animals, including subhuman primates, which would deliver highly localized electrical stimulation into the target nucleus, and which would include the capability of monitoring the response to the electrical stimulation by individual neurons in the target nucleus. These capabilities may prove useful in a clinical device, with the additional requirement that the microelectrodes must deliver the stimulation for an extended interval, without injury to the tissue. An array of independently controllable stimulating microelectrodes distributed throughout the target nucleus would permit precise control of the spatial distribution of the stimulation, by stimulating either with single microelectrodes or with a subgroup of microelectrodes that could be pulsed either simultaneously or sequentially.

Manuscript received February 1, 2005; revised July 17, 2005. This work was supported in part by the National Institutes of Health (NIH) under Research Grant NS40860-02. *Asterisk indicates corresponding author.*

*D. McCreery is with Huntington Medical Research Institutes, Neural Engineering Program, 734 Fairmount Ave., Pasadena, CA 91105 USA (e-mail: dougmc@hmri.org).

A. Lossinsky, V. Pikov, and X. Liu are with Huntington Medical Research Institutes, Neural Engineering Program, Pasadena, CA 91105 USA.

Digital Object Identifier 10.1109/TBME.2006.870215

II. Methods

Fig. 1(A) shows an example of our deep brain microelectrode array. The entire array assembly is 16 mm in length and 2 mm in diameter. It includes a 6-mm stainless-steel (type 316L) alignment cylinder and 16 iridium microelectrodes, each 5 to 6 mm in length, comprising a fascicle that is 1.8 mm in diameter. While the length of the microelectrodes is greater than what is required for the animal model in which it was developed (STN of the adult domestic cat), we have developed the device with an eye toward its eventual clinical use in the human STN and the internal segment of the globus pallidus, which are much larger than their counterparts in the domestic cat. The fascicle of iridium microelectrodes extends from a cap of EpoTek 301 epoxy, a material that carries a USP Category VI certification for chronic implantation.

The shafts of the discrete iridium microelectrodes are formed from iridium wire, 75 μm in diameter. In a 3-step process, one end of each shaft is etched electrolytically to a cone having an included angle of approximately 8°. The cone terminates in a blunt tip with a radius of curvature of 5–6 μm. The blunt tip allows a more uniform distribution of the stimulus current over the exposed surface [7] and induces minimal tissue damage during chronic implantation into the feline cochlear nucleus [8]–[10]. A wire lead (platinum-10% iridium, 25 μm in diameter) is microwelded near the upper end of the shaft. The microelectrode shafts and wire are insulated with 3 μm of Parylene-C and the insulation is ablated from the tips of the shafts, using an excimer laser operating at 248 nm. The surface areas thus exposed ranged from approximately 500 μm^2 to 2 000 μm^2 [Fig. 1(B)].

The individual microelectrodes are assembled into a fascicle of 16 with a center-to-center spacing of 350 μm. A custom fixture holds the microelectrode shafts in alignment and also serves

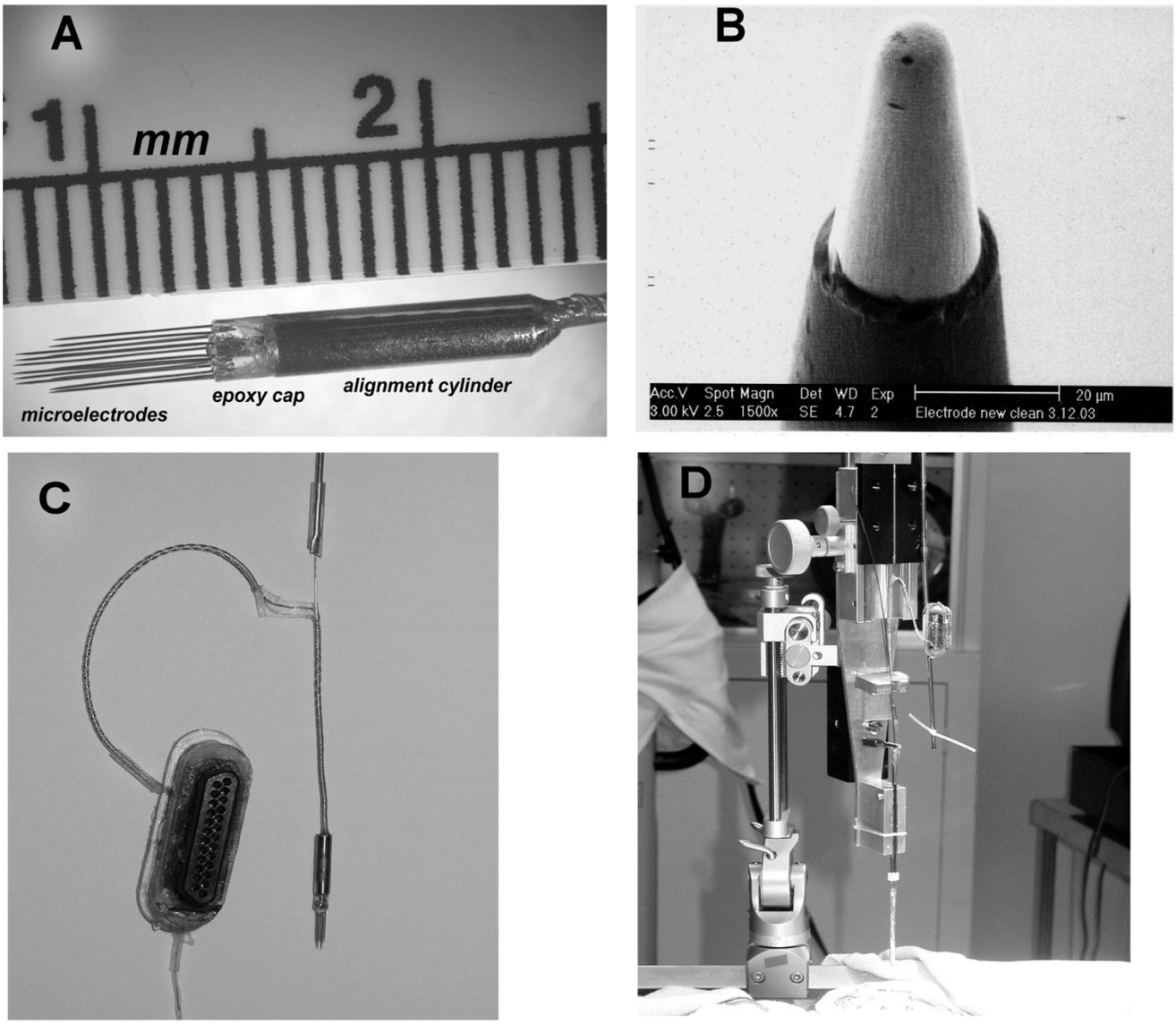

Fig. 1. (A) The deep brain microelectrode array. (B) A scanning electron micrograph of the tip of one of the iridium microelectrodes. The exposed iridium metal appears light, the Parylene insulation dark. (C) The array and cable with the stiffening pin inserted into the cable lumen. The percutaneous connector also is shown. (D) A Photograph of the apparatus for implanting the array into the deep brain. The inserter is mounted on a standard stereotaxic electrode carrier.

as a mold for casting the epoxy cap. The fascicle is composed of two concentric rings of microelectrodes, those in the inner ring being approximate 1 mm longer than in the outer ring. Two microelectrodes are omitted from the outer ring. This gap, and the differences in the lengths of the microelectrodes, allows for each of the tip sites to be identified in the histologic sections, as described below.

The 16 lead wires are spiraled around a section of silicon tubing 0.5 mm in diameter and the windings are overlaid with a layer of Med A silicone elastomer, to form a cable that terminates in a percutaneous connector. During implantation, a steel stylet is inserted into the lumen of the silicon tubing. When the stylet is withdrawn, the cable is sufficiently flexible to allow the implanted array to move with the brain. Fig. 1(C) shows an array, the cable with the stylet inserted, and the percutaneous connector.

The microelectrodes are "activated" (a film of polyvalent iridium oxide is formed) by potentiodynamic cycling between -0.6 and $+0.8$ V with respect to an Ag/AgCl electrode, with the microelectrodes immersed in saturated sodium phosphate solution. The activation continues until the electrodes have a total charge capacity of approximately 25 mC/cm^2. The charge capacity of iridium oxide ("activated iridium") is very high, [11], [12] allowing the microelectrode's surface area to be sufficiently small such that action potentials can be recorded from single neurons, yet have adequate charge capacity for prolonged microstimulation. The arrays are then cleaned using the "modified Clemson protocol" [13] and sterilized in ethylene oxide, in preparation for implantation.

Aseptic technique and general anesthesia were used during implantation of the arrays into deep brain structures of 11 young adult cats of either sex (age 10 mo-2 years). The animal's head was fixed in a stereotaxic apparatus, the scalp and temporalis muscle were reflected and a small craniectomy (approximately 6×6 mm) was made over the right cerebral cortex. The apparatus for implanting the array into the deep brain is shown in Fig. 1(D). It is mounted on a standard microelectrode carrier, on the stereotaxic head frame. Fig. 2(A)–(E) depicts the sequence for implanting

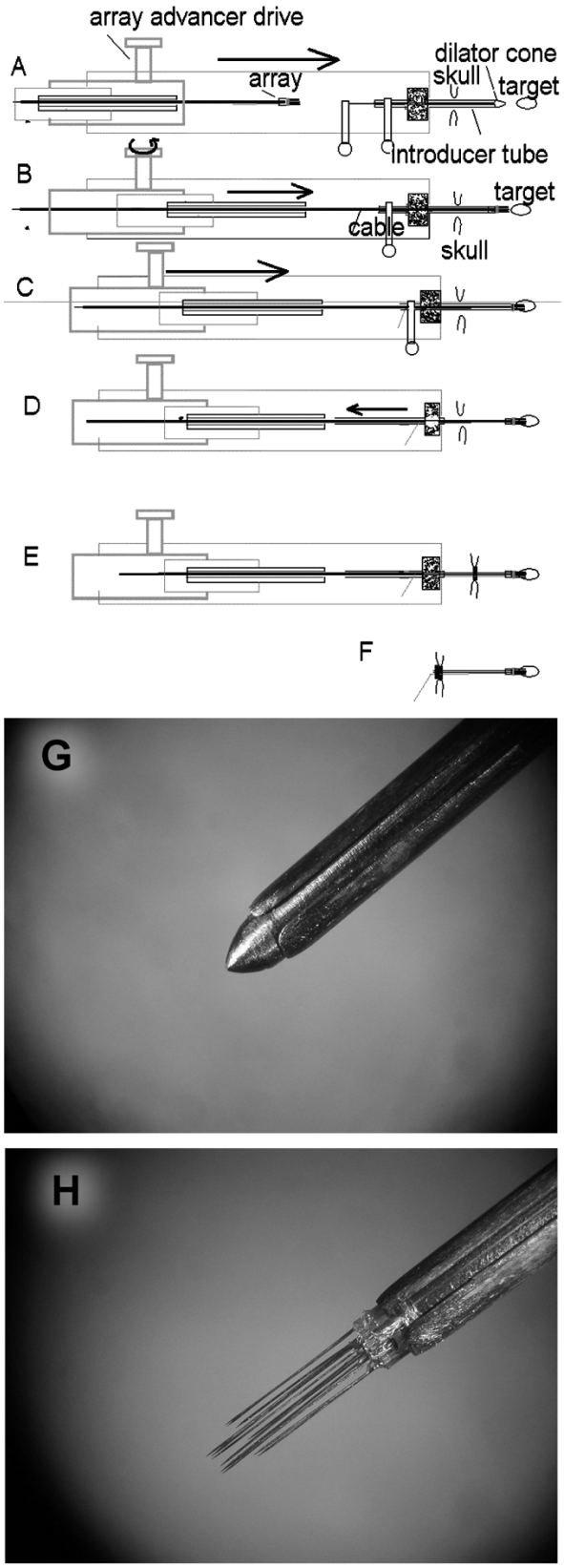

Fig. 2. (A)–(F) Sequence of steps for implanting the array using the apparatus shown in Fig. 1(D) (see text for details). (G) The tissue dilator cone protruding from the orifice of the slotted introducer tube. (H) The dilator cone has been retracted and replaced by the microelectrode array.

the array into the cat's deep brain. The procedure is designed to prevent the brain tissue from being raked by the fascicle of microelectrodes, and also to protect the microelectrodes until they are close to the target. The introducer apparatus is advanced by the stereotaxic drive [Fig. 2(A)], and the slotted introducer tube, with a tissue dilator cone protruding from the orifice [Fig. 2(G)], is passed through a slit in the dura and a small nick in the pia, and advanced into the brain in steps of 1 mm, at 2 steps per minute, to within a few millimeters of the target. The dilator cone is then withdrawn and the microelectrode array, supported by the steel stylet within the cable, is guided into the introducer tube by a rack-and-pinion drive until the electrode shafts protrude fully from the end of the tube [Fig. 2(B), (H)]. Next, the entire assembly is advanced a few millimeters so that the electrode tips enter their target [Fig. 2(C)]. The array's elongated alignment tube ensures that the microelectrodes are kept aligned with the long axis of the introducer, and this reduces the risk of slashing the tissue. The introducer tube is then retracted out of the brain. The stylet within the cable prevents the array from retracting as the introducer is withdrawn [Fig. 2(D)]. The burr-hole is filled with a thin layer of gelfoam and then with bone cement [Fig. 2(E)] and when the cement is cured, the stylet is withdrawn. [Fig. 2(F)]. The cable terminates in a 25-pin percutaneous connector, which is attached to the skull with stainless-steel screws and bone cement.

Most of the arrays were implanted into the STN, at stereotaxic coordinates A7.5, R6.4, and with the electrode tips approximately 3 mm below the interaural line. The array is introduced vertically (in the parasagittal and frontal planes). Final adjustment of the vertical coordinate is aided by intraoperative monitoring of neuronal activity. In normal adult cats, the STN can be recognized by well-resolved neuronal units with discharge rates of 15–25 pulses per second, and relatively high background "noise" due to unresolved neuronal activity.

For microstimulation in the STN, the waveform was charge-balanced, cathodic-first pulse pairs, 150 μs/phase in duration. The controlled-current stimulator is isolated from the recording amplifier by a radio frequency link, to eliminate ground loops and reduce stimulus artifacts. This allows us to stimulate through one microelectrode and to record neuronal action potentials via an adjacent microelectrode.

Recordings of neuronal activity and short-term stimulations were performed with the cat unanesthetized. In most cases, the cats were lying on the technician's lap, to avoid becoming entangled in the tethering cable. Extracellularly recorded action potentials (spikes) were amplified 2500 times and bandpass filtered at 100 Hz to 8 KHz using a custom-build 16-channel amplifier and digitized into a computer at 25 000 samples per second using a 16-channel data acquisition board (National Instruments PCI-6070E). The recordings were processed offline through a software digital filter with a band pass of 500 Hz–5 KHz. An amplitude distribution histogram of all positive and negative peaks were generated and from this, a histogram of the noise component was generated, assuming a Gaussian amplitude distribution of the noise peaks. Spikes were detected as events whose amplitude was at least 3 times the standard deviation of the noise distribution. From these events, and the responses to 1500 successive stimulus pulses, poststimulus time histograms with a bin width of 1 ms were constructed.

The prolonged stimulations were conducted using a 16-channel controlled- current simulator housed in a back-

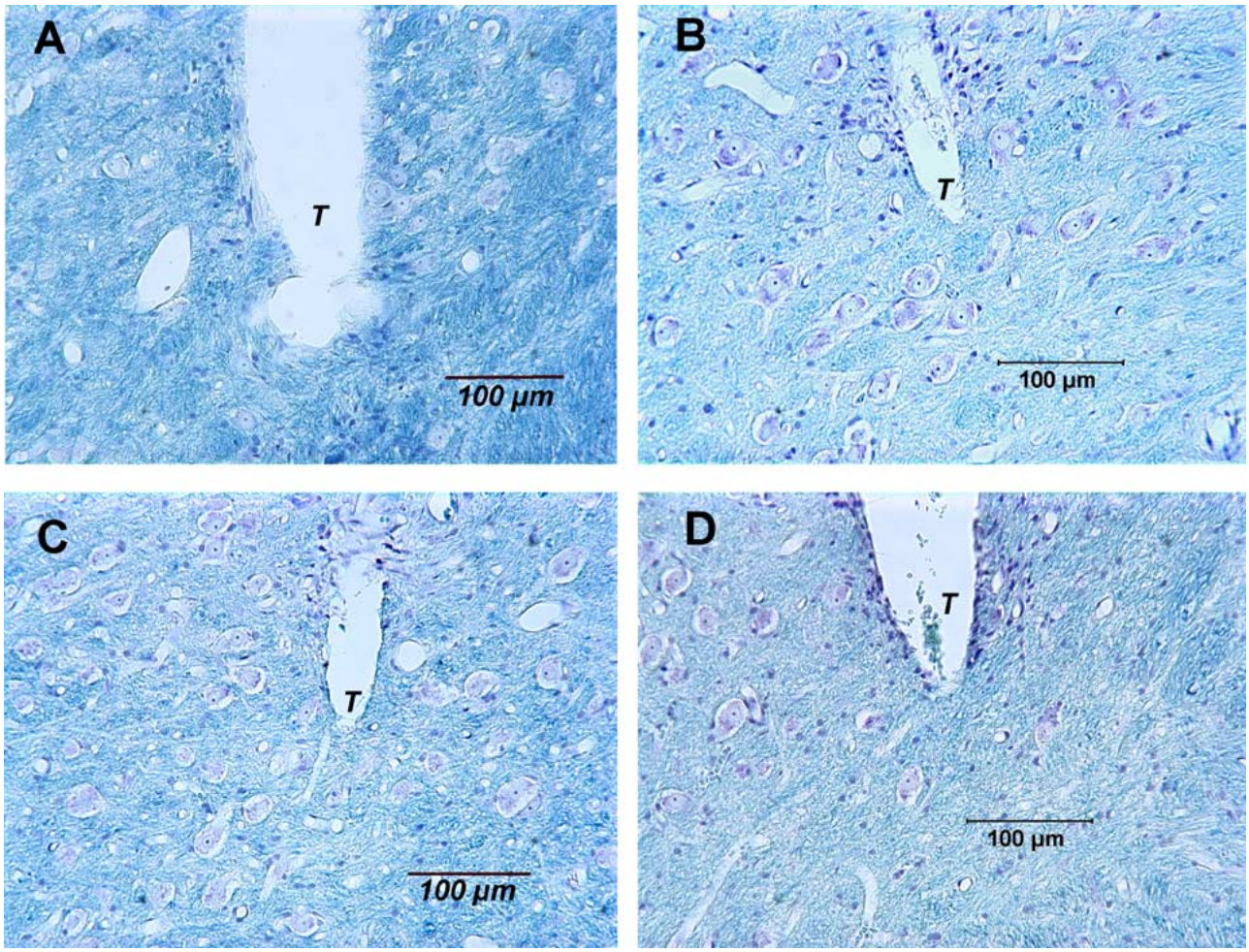

Fig. 3. The tip sites of 4 microelectrodes implanted in cat DB2 for 294 days. The neurons and neuropil adjacent to the tip sites (T) appear normal (Luxol fast blue and Cresyl violet).

pack and controlled from a computer via an RF telemetry link. During the stimulation, the cats could move about freely in a large acrylic cage. The backpack module also contained a downlink transmitter that permitted continuous monitoring of the voltage transients induced across the microelectrodes by the controlled current stimulus pulses.

For histologic evaluations of the implant sites, the cats were deeply anesthetized with pentobarbital and perfused through the ascending aorta with 1 liter of phosphate-buffered saline prewash followed by 3 liters of phosphate-buffered 4% formalin solution. Twenty-four hours later, the array was withdrawn and a block of brain containing the lower part of the array's alignment cylinder and the electrode shafts was resected and embedded into paraffin. The tissue was sectioned at a thickness of 8 μm, approximately in the frontal plane and approximately parallel to the electrode shafts. The boundaries of the STN are most easily visualized when the tissue is sectioned in the frontal plane. The tissue sections were stained with Luxol Fast Blue to highlight axons and neuropil and counterstained with Cresyl Violet (Nissl stain) to visualize cell bodies. The site of each of the 16 microelectrode tips was photographed with a digital camera and these images were used to reconstruct a face-on view of the array's footprint using a MatLab script. The gap in the outer ring of microelectrodes can be identified in this face-on view so that the identity of each of the microelectrode tip sites is established.

III. Results

Eleven arrays have been implanted into 11 adult cats. The first array was implanted into the internal segment of a cat's the left globus pallidus and the next 10 were targeted to the right STN. In all cases, the animal's postsurgical recovery was uneventful. All cats were sacrificed for histologic evaluation of the implant sites at 140–415 days after the implant surgery. Some experience was required in order to strike the small feline STN and in 2 of the first 3 animals, the array was implanted slightly rostral of its target. In 8 of the 10 cats in which the array was targeted to the STN, and for which histologic data are available, some of the microelectrode tips were in the STN.

The feline STN is bounded ventrally and laterally by the cerebral peduncle and dorsally by the zona inserta. Fig. 3 shows the tip sites of the 4 microelectrodes in cat DB2 that were located within the STN. The plane of the histologic sections is slightly oblique to the axis of the microelectrodes, causing the terminus of each microelectrode track to appear as an ellipsoid. This cat was sacrificed 294 days after the implant surgery, but the gliotic sheaths around the microelectrodes were only a few microns in thickness, and the surrounding neurons and neuropil appear normal.

Fig. 4(A) shows a section through the center of the epoxy button, at the transition from the array's superstructure to the

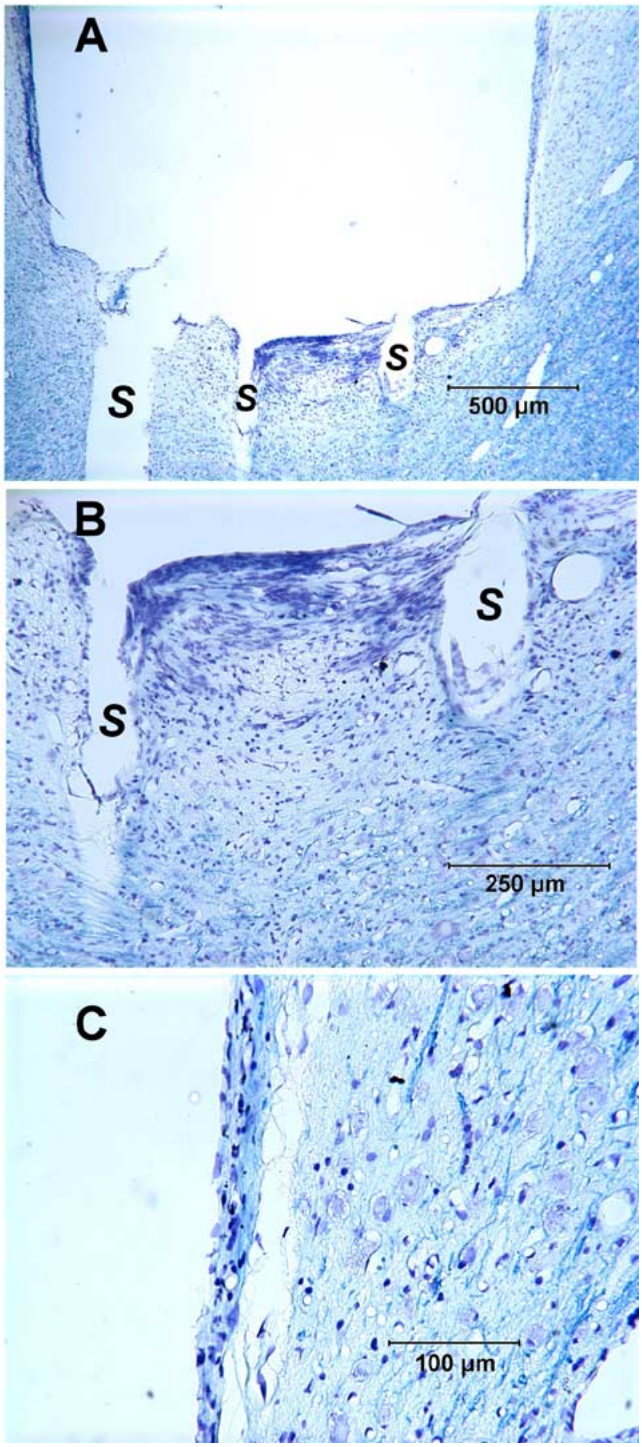

Fig. 4. Micrographs of the tissue adjacent to the array's supporting structures, from cat DB2. (A) A section through the center of the site of the epoxy button, showing the upper end of 3 of the microelectrode shafts (S). (B) A view at higher magnification of the tissue subjacent to the epoxy button. (C) The tissue adjacent to the stainless-steel alignment cylinder (cyl).

fascicle of microelectrodes [see also Fig. 1(A)]. Fig. 4(B) shows the tissue subjacent to the underside of the button, at higher magnification. Here, the gliosis is more extensive than around the individual microelectrode shafts and tip sites (Fig. 3), but neurons and neuropil 1 mm beneath the epoxy button appear normal. This demonstrates good preservation of tissue in the midst of the fascicle of microelectrode shafts. Fig. 4(C) shows the tissue adjacent to the side of the stainless-steel alignment tube. The glial sheath is quite thin (approximately 25 μm). However, many of the neurons within approximately 300 μm of the tube, while recognizable, are somewhat shrunken. Neurons 300 μm or more from the alignment tube appear normal. The results from 8 other cats were similar. In one animal (DB7), inflammatory cells were seen around some of the microelectrode shafts, apparently due to an undetermined contamination of the Parylene insulation.

In all 11 cats, we were able to record the action potentials of single neurons in and around the STN, and in cat DB1, from the globus pallidus. Fig. 5(A)–(E) shows neural activity recorded from 5 cats at 220–340 days after array implantation. The responses shown in Fig. 5(A) were from the microelectrodes whose tip sites are shown in Fig. 3. The surface areas of the electrodes were 500 ± 150 μm^2 in cat DB9, $1\,000 \pm 200$ μm^2 in cats DB2, DB10, and DB11, and $2\,000 \pm 300$ μm^2 in cat DB8. Rather unexpectedly, the quality of the unit recordings was not significantly poorer when the electrode surface areas were larger, although the microelectrodes with the large exposed tips tended to record multiple, rather than single, neuronal units. Fig. 5(F) is a plot of the number of channels in each of the 11 cats from which we were able to record action potentials with signal-to-noise ratios (SNRs) of 3 or greater (S/N = Mean peak spike amplitude/RMS noise amplitude). We could record from an average of 4 to 5 microelectrodes in each cat, throughout the period of implantation. In three cats (DB5, 6, 7), we were not able to record action potentials with good S/N from any of the microelectrodes. The temporal grouping of these 3 implants is suspicious, but we have been unable to identify a particular reason for the failure. In the other cats, the number of channels from which we could record action potentials varied over time, but showed no clear trend.

An important feature of our array is its ability to stimulate in the STN and record neuronal activity via the same set of microelectrodes. Fig. 6(A) is a diagram of the face-on view of the array implanted in the cat DB2, showing the relative position of the 4 microelectrodes in the STN [the tip sites of these microelectrodes are depicted in Figs. 3(A)–4(D)]. Fig. 6(B) shows the location of the tips of the 4 microelectrodes, all projected onto a histologic section near the caudal end of the electrode fascicle (the terminus of the track of microelectrode #16 is seen in this section). The tip sites are clustered in the lateral and dorsolateral part of the nucleus, the portion that is associated with motor circuits, so this animal best illustrates the interaction of stimulation and recording sites along the rostral-caudal dimension of the nucleus. In all cases, the stimulus was biphasic pulse pairs, 26.5 μA in amplitude and 150 μ s/phase in duation.

Our recording system does not permit simultaneous recording and stimulation through the same microelectrode. However, we were able to record via the adjacent microelectrodes, 350 μm distant, and in a few instances, we were able to record the direct response of the neurons to the stimulus pulse [Fig. 6(C)]. In most cases we were able to record delayed responses while stimulating with one microelectrode and recording with another. These responses are illustrated by the poststimulus time (pst) histograms of the single-unit neuronal activity [Fig. 6(D)–H]. We compared the pst histograms shown in Fig. 6 (and, also, in Fig. 7) with those generated without the stimulation, using a chi-squared test for

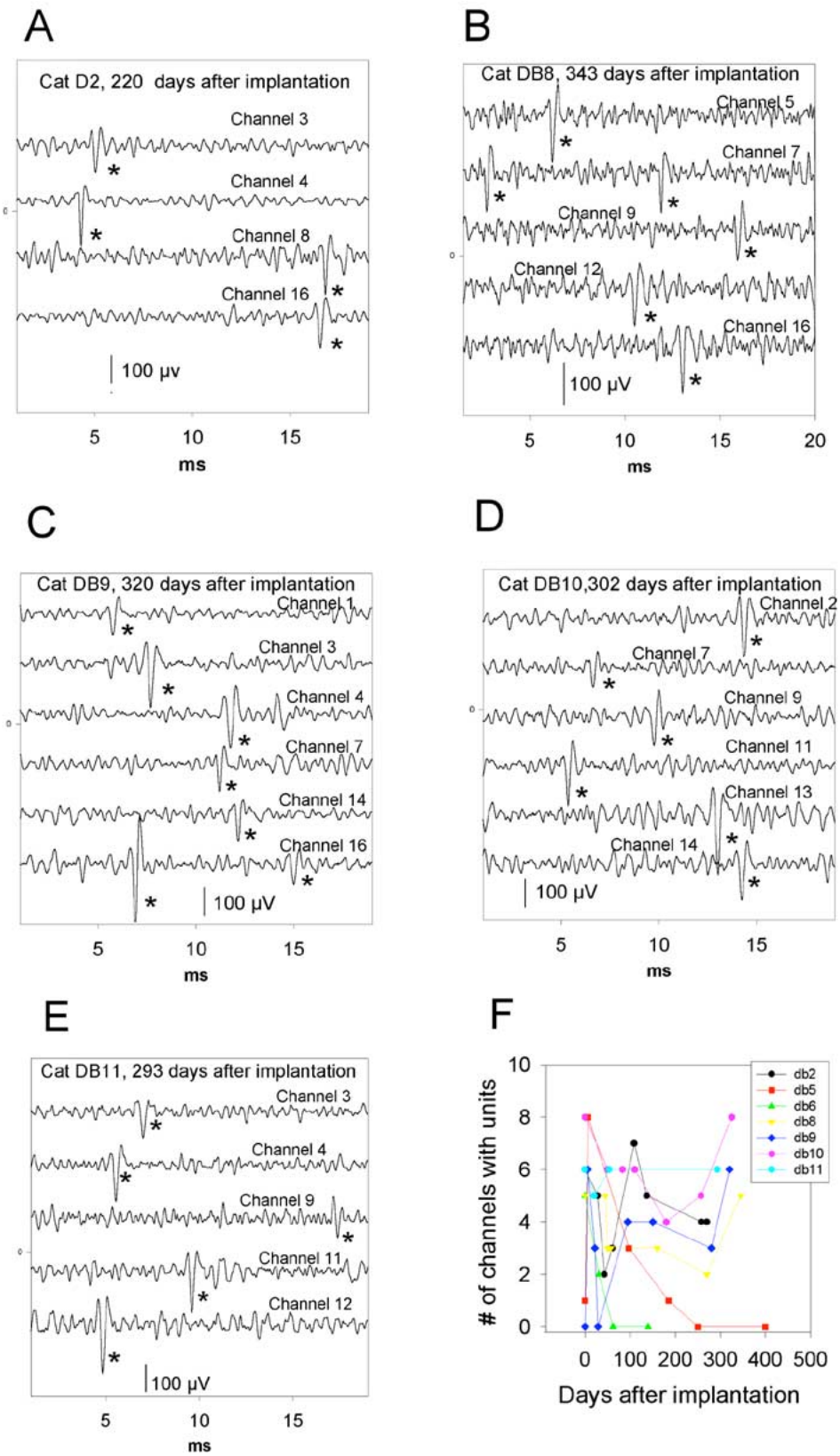

Fig. 5. (A)–(E) Extracellular action potentials (∗) recorded in 5 cats at 228 to 343 days after array implantation. The 4 channels of data from cat DB2 are from the electrodes whose tip sites are shown in Fig. 4. The electrode surface areas were approximately as follows: A, D, E $= 1\,000\,\mu\text{m}^2$, C $= 500\,\mu\text{m}^2$, B $= 2\,000\,\mu\text{m}^2$. (F) The number of microelectrodes in each of the 11 cats from which we were able to record action potentials with SNRs of 3 or greater (S/N= Mean peak spike amplitude/RMS noise amplitude). The plots end at the time the cats were sacrificed, except for DB11, which remains alive.

goodness of fit. In all cases, the histograms generated with the stimulation were significantly different from those without stimulation $(\text{P} < .01)$, showing that the stimulus produced significant modulation of the temporal distribution of action potentials. The most common response to the stimulus was a burst of 2 or more action potentials peaking 8–12 ms after the stimulus pulse. These

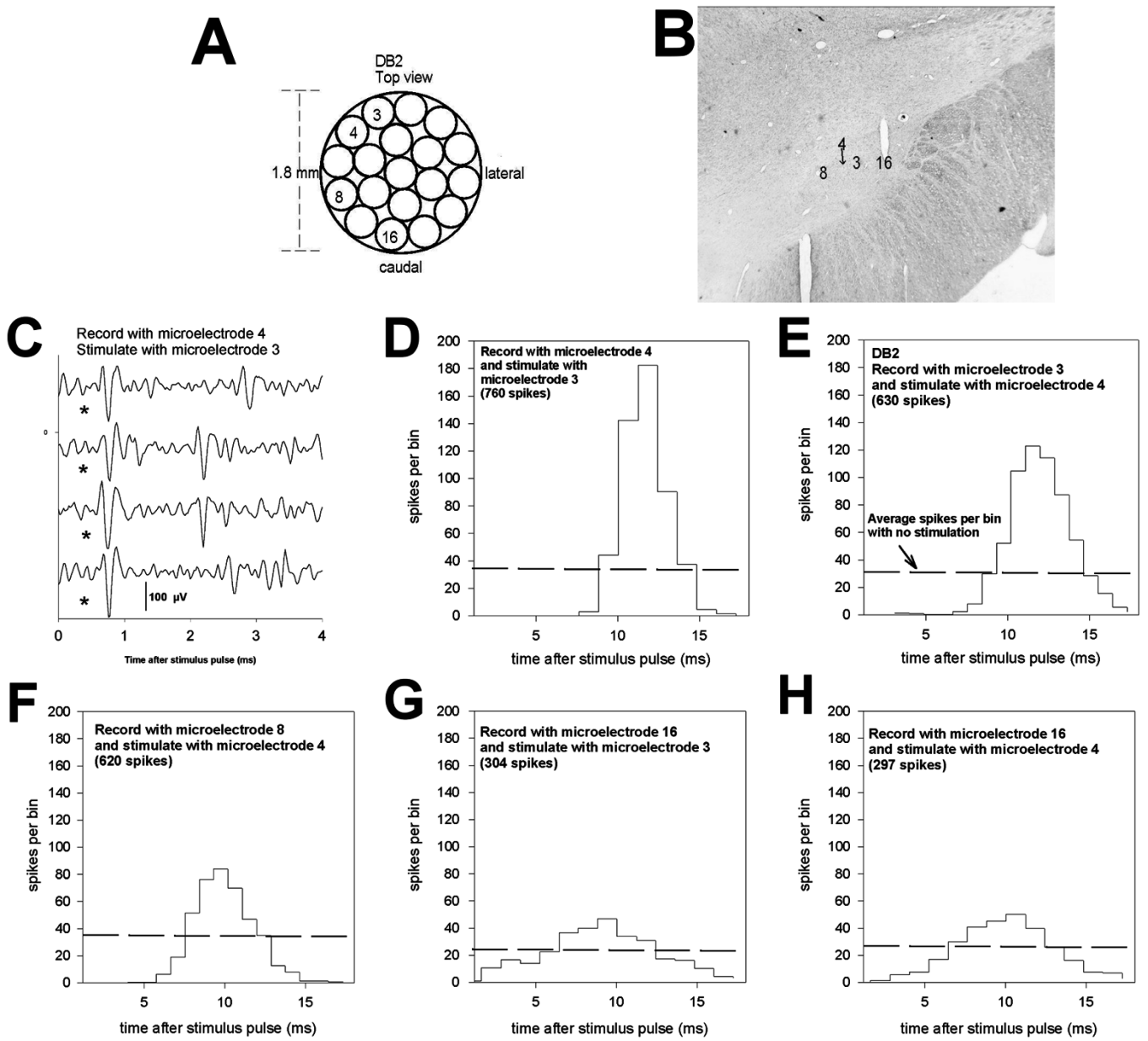

Fig. 6. (A) A diagram of the microelectrode fascicle from the array implanted into cat DB2, seen in a face-on view. (B) The location in the subthalamic nucleus of the tip sites of the 4 microelectrodes depicted in (A). Note that the views in (A) and (B) are at right angles to one another. The tip sites are projected onto one histologic section in the frontal plane and through the subthalamic nucleus (Cresyl violet stain). (C) Samples of the actions potentials recorded at microelectrode site 4 while stimulating at adjacent site 3. The neural unit (∗) responded to the stimulus at short and constant latency. (D–H) Poststimulus time histograms of the activity of single neural units recorded at the sites depicted in (A) and (B) while stimulating at other sites. The action potentials shown in (C) and the histogram shown in (D) were from different neural units, and the data were recorded on different days. In all cases, the stimulus was 26.5 μA current pulses, at 50 Hz. The histograms were generated from the responses to 1500 successive stimulus pulses. In each frame, the broken horizontal line indicates the average firing rate of the unit without stimulation. (See text for details)

were temporally dispersed after the stimulus, indicating that they were induced transynaptically. In most cases, the units' average firing rate was little changed, and the effect of the stimulation was to partially entrain the action potentials. The entrainment effect was strongest when the stimulating and recording microelectrodes were close together. Thus, Fig. 6(D), (E) shows the strong mutual excitation when stimulating and recording at a pair of adjacent sites (sites 3 and 4, separated by 350 μm). Fig. 6(F), (G), (H) show the somewhat weaker entrainment of the action potentials between sites 8 and 4, that were separated by approximately 700 μm [Fig. 6(F)] between sites 16 and 3, separated by about 1500 μm [Fig. 7(G)], and between sites 16 and 4 [Fig. 6(H)], separated by about 1400 μm.

Fig. 7(A) shows the relative positions of 3 microelectrodes whose tips were in the STN of cat DB6. Fig. 7(B) shows the locations of the tips in the STN, projected onto a histologic section through the most rostral of the microelectrode tracks (microelectrode 10). These microelectrode sites are more widely dispersed in the medio-lateral dimension than those in cat DB2. Thus, microelectrode 10 was on the dorsal margin of the STN, microelectrode 12 in the extreme lateral part of the nucleus, and microelectrode 11 near its medial margin. Stimulating at site 11,

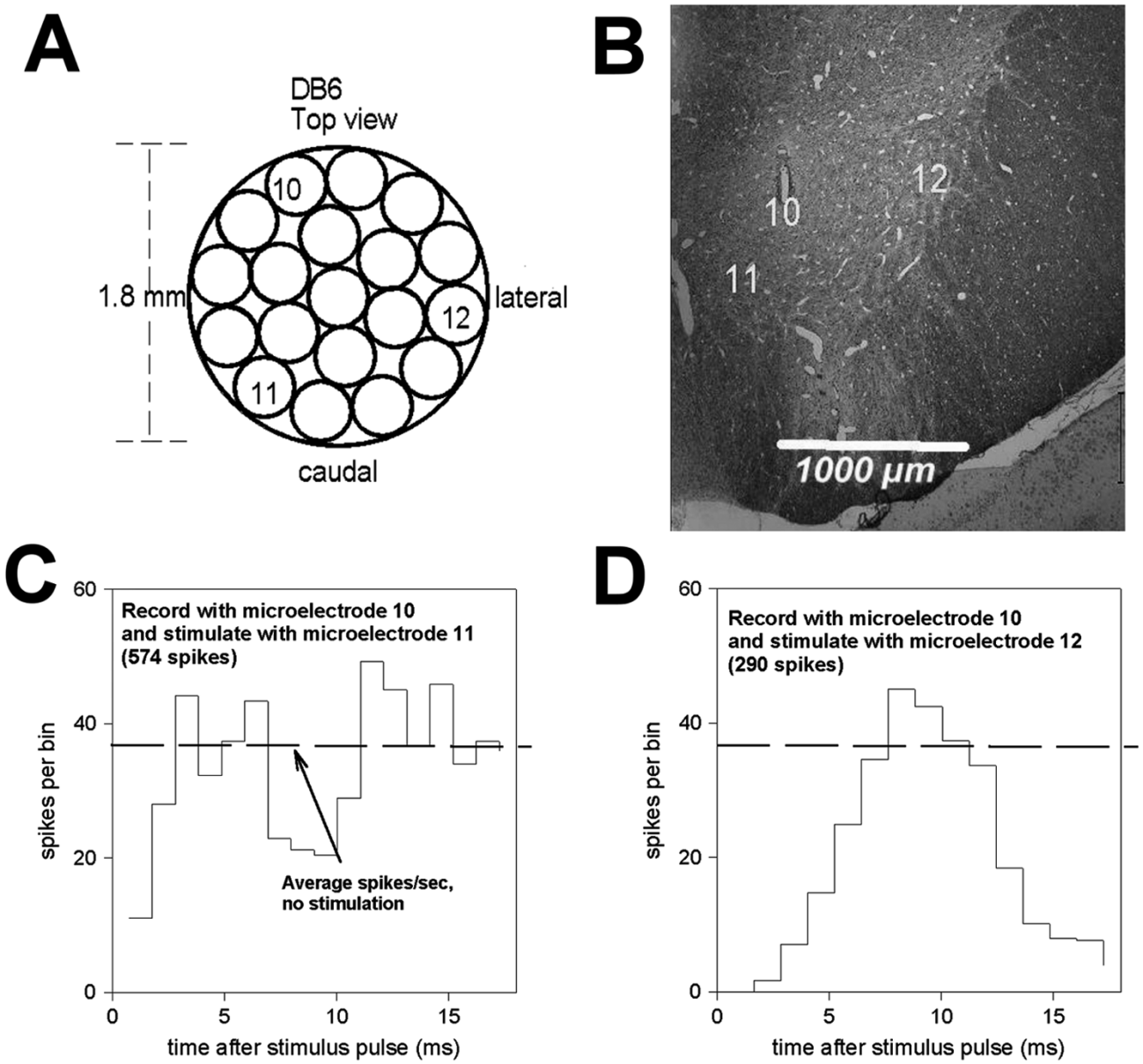

Fig. 7. (A), (B) The location of 3 microelectrode tips in the subthalamic nucleus of cat DB6. (C), (D) The poststimulus time histograms of the response of a single neural unit recorded at site 10 while stimulating at either of the other 2 sites.

at 26.5 μA, produced a small notch (apparently a transient inhibition) in the pst histogram [Fig. 7(C)]. We are unaware of any studies demonstrating intrinsic inhibitory neurons in the STN, but many studies have shown that the nucleus receives inhibitory (GABA-ergic) afferents from extrinsic sources, primarily from the external segment of the globus pallidus, and these pathways are well developed in the cat [14], [15]. When the stimulus was applied at site 12 [Fig. 7(D)], near the medial margin of the STN, the neural unit recorded at site 10 [approximately 1 000 μm distant; Fig. 7(A), (B)] exhibited a modest entrainment of the actions in a manner similar to that seen in cat DB2. Similar results were obtained from 2 other cats (DB4 and DB5).

Figs. 6 and 7 illustrate how microstimulation in the STN at an amplitude of 26.5 μA (4 nC/ph) using 150 μs biphasic cathodic-first, controlled-current pulse pair can effectively excite the intrinsic neurons of this nucleus. We then determined the effect of prolonged intranuclear microstimulation using the same parameters. In each of 3 cats, a subset of the chronically implanted microelectrodes was pulsed for 7 hours per day on 5 successive days. Since high-frequency stimulation in the STN has been shown to most effectively ameliorate the symptoms of Parkinson's disease, we used a stimulus pulse rate of 100 Hz. Four microelectrodes in cats DB8 and DB9 were pulsed, and 5 were pulsed in DB10. None of the animals exhibited any behavior response to the stimulation. The animals were perfused 24 hours after the last session of stimulation. The active surface areas at the tips of the microelectrodes differed in these animals, being approximately 2 000 μm^2 in DB8, 500 μm^2 in DB9, and 1 000 μm^2 in DB10. Thus, while the stimulus charge per phase was invariant, the charge density differed and was approximately 200 $\mu C/cm^2$ in DB8, 800 $\mu C/cm^2$ in DB9, and 400 $\mu C/cm^2$ in DB10.

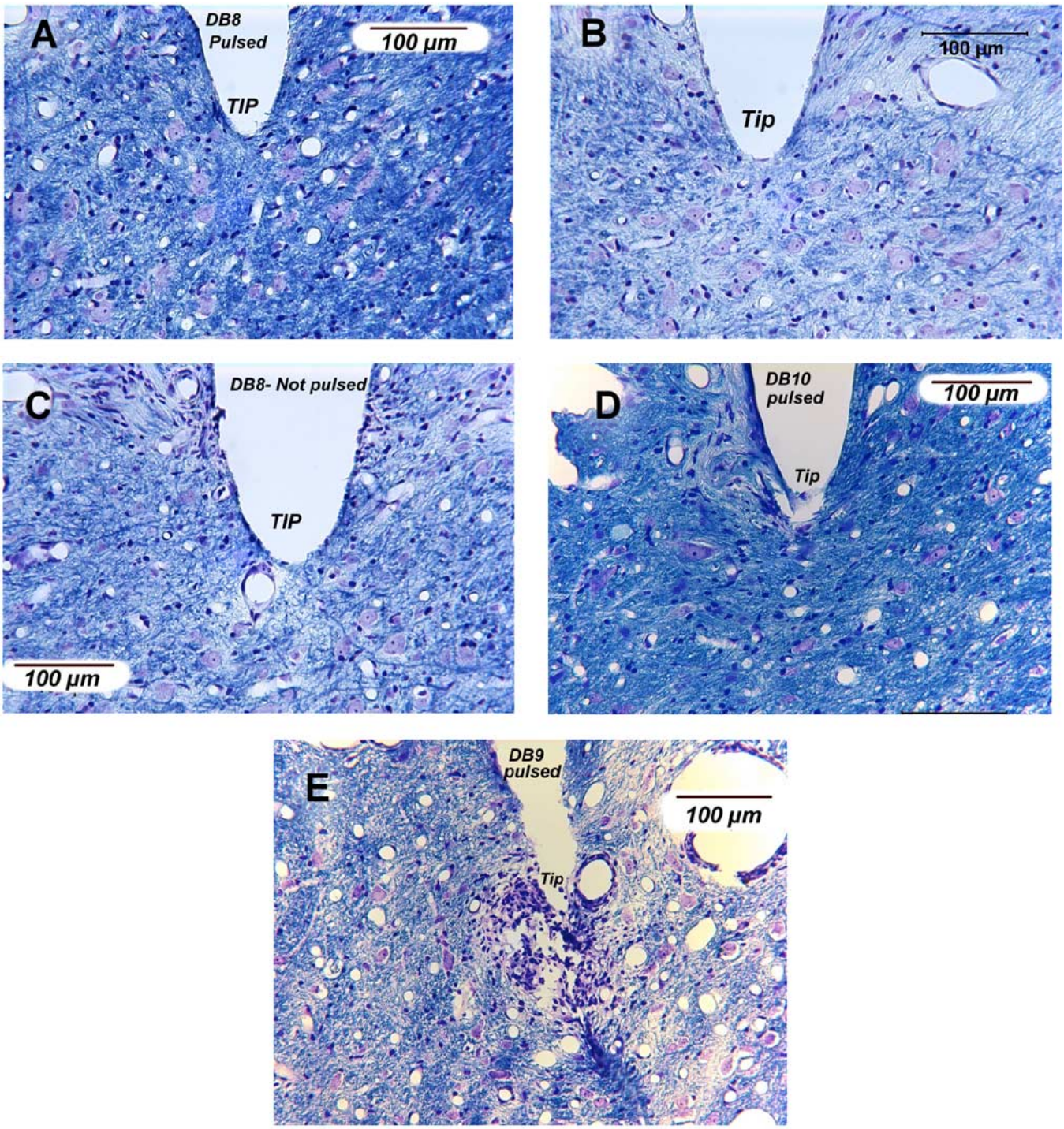

Fig. 8. Histologic sections through the tip sites of microelectrodes in the subthalamic nucleus of 3 cats. The sites labeled as pulsea (A), (B), (D), and (E) had received 7 hours of stimulation at 100 Hz and 4 nC/phase, on 5 successive days. The charge density varied across animals due to the differences in the microelectrodes' surface areas, and were approximately as follows: A, B $= 200\ \mu$C/cm^2, D $= 400\ \mu$C/cm^2, E $= 800\ \mu$C/cm^2. See text for details. (Luxol fast blue with Cresyl violet.)

Fig. 8(A), (B) shows the tip sites of 2 of the 4 pulsed microelectrodes from cat DB8. Fig. 8(C) shows an unpulsed tip site from the same animal. The neurons and neuropil at the 4 stimulated sites appeared normal, and are indistinguishable from the unstimulated sites. The 5 stimulated sites from cat DB10 also appear normal; one site is shown in Fig. 8(D).

Fig. 8(E) shows the tip site of 1 of the 4 pulsed microelectrodes from cat DB9. All 4 of the pulse sites from this cat were surrounded by aggregates of inflammatory cells (from their morphology, probably macrophages). The charge density in cat DB9 was higher than in the other animals (approximately 800 μC/cm^2).

IV. Discussion

The objective of this study has been to develop a chronically implantable microelectrode array in which the spatial density

of the microelectrodes is sufficient to allow close control of the spatial distribution of the stimulus.

Numerous studies have demonstrated a topographic organization of the afferent and efferent projections to and from the STN of many species [16]–[23]. On the basis of the reciprocal connections between the STN and the cerebrum, the broadest topographic subdivision appears to be between motor, association and limbic functions. However, there is ample evidence for finer subdivisions of the topology, including a somatotopic mapping of motor functions in humans. It is quite possible that a clinical device that can access this topology will allow for greater flexibility in the treatment of motor disorders than is possible with the deep brain arrays now in clinical use. These use macroelectrodes, and the electrical stimulation tends to spread quite broadly. McIntyre *et al.* [24] modeled the current field that is induced by the stimulus parameters typically used to ameliorate the symptoms of Parkinson's disease, and found that the effective stimulus may extend well beyond the boundaries of the STN. They suggested that this may account for some of the side effects that often accompany deep brain stimulation in the STN, including tetanic muscle contraction, speech disturbance and ocular deviations [25].

We have developed a microstimulating device that can be implanted chronically into the deep brain. There was remarkably little tissue injury in the vicinity of the fascicle of 16 microelectrodes. The tissue responses shown in Fig. 3 are typical of all tip sites of the unpulsed microelectrodes. All of the microelectrode tips were surrounded by thin gliotic sheaths 5–15 μm in thickness. The density of the neurons in the vicinity of the tip sites varied according to the tip's location in the STN. We did not perform a quantitative analysis of neuronal density around the tip sites, but there was no suggestion that the neuronal density surrounding the electrode tips was reduced. Small gliotic scars, 40 to 60 μm in diameter, sometimes were seen adjacent to one side of the tips of the microelectrodes [e.g, Fig. 9(D)]. In the 9 cats for which histology is available, we found no areas of infarction or evidence of hemorrhages or hematomas.

In most cases, we were able to record single neuronal action potentials from at least some of the microelectrodes, for the duration of the implant (up to 435 days), using microelectrodes with tip areas of 500 to 2 000 μm^2 (Fig. 6). Thus a tip area of 1 000 to 2 000 μm^2 appears to be appropriate for microelectrodes that are to be used for both prolonged stimulation and recording of neuronal activity. This will allow prolonged, nondamaging stimulation at an amplitude of at least 4 nC/ph, which is adequate to excite the neurons in the STN. Within the range of tip sizes between 1 000 to 2 000 μm^2, there will be a tradeoff between the maximum safe amplitude of prolonged microstimulation and the ability to resolve the action potential of single neurons.

We have identified stimulus parameters that can safely excite the neurons of the feline STN during a regimen of prolonged stimulation. We found that a stimulus of 4 nC/ph (26.4 μA biphasic current pulses, 150 μs/ph in duration) was sufficient to directly excite the neurons of the feline STN, and this stimulus also could modulate the activity of these neurons over a considerable distance within the STN, possibly by excitation of afferent axons that make synapses upon the neurons of the STN. It remains to be determined if this somewhat widely distributed transsynaptic effect of the intra-nuclear microstimulation, illustrated in Figs. 6 and 7, would be useful in the clinical treatment of movement disorders or more generally, what the clinical role of highly localized microstimulation in the treatment of movement disorders might be. However, we have demonstrated that prolonged, high-rate microstimulation can be applied in the STN without histologically detectable injury to the adjacent neurons and neuropil.

In the feline cochlear nucleus, stimulation-induced neural damage is manifested as vacuolations of the large myelinated axons that characterize the neuropil of this nucleus [9]. The threshold for this type of injury is approximately 3 nC/phase and is relatively independent of charge density for iridium microelectrodes of the same range of surface areas as those used in the present study (500–2 000 μm^2). The charge per phase used in the present study (4 nC/ph) was slightly above the level at which the vacuolations were observed in the feline cochlear nucleus. These vacuoles were not seen in the feline STN or in the feline cerebral cortex stimulated with similar parameters, and their presence in the feline cochlear nucleus may simply be a consequence of the predominance of large myelinated axons in that structure. However, in the STN, we noted a different phenomenon; namely, a dense aggregate of inflammatory cells (from their morphology, apparently mostly macrophages) around the tips of some of the pulsed microelectrodes. We previously have observed these aggregates around pulsed microelectrodes implanted in the feline spinal cord [26] and in the cerebral cortex. In the STN, the aggregates of inflammatory cells were seen around microelectrodes pulsed at 800 $\mu C/cm^2$ and 4 nC/ph, but not at 500 $\mu C/cm^2$. While the significance of these aggregates to the viability and functionality of the neural substrate is unclear, we prefer a conservative criterion for safety of electrical stimulation; namely, that the stimulus should induce no histologically detectable changes in the tissue. On this basis, we tentatively define the upper limits for safe microstimulation in the feline STN to lie between 500 and 800 $\mu C/cm^2$ at 4 nC/ph. This criterion can be met by using microelectrodes having surface areas of 1 000 μm^2 or greater. We were able to record the action potentials from single neurons in the STN with microelectrodes having surface areas of at 500 to 2 000 μm^2. Thus, by judicious selection of the microelectrode' active area, the microelectrodes can be used both for microstimulation and for recording of neuronal activity, with the caveat that the larger electrodes are more likely to record multi-unit activity. Microelectrodes with larger surface areas would permit safe stimulation at a greater charge per phase and thus through a larger volume of tissue, while still allowing much greater localization of the stimulus than is possible with the arrays now in clinical use. The function of recording single-unit action potentials would then have to be relegated to other microelectrodes with smaller surface areas, if such a capability capacity is deemed to be of value in a clinical device, either as an aid in the positioning of the array, or subsequently, as an aid to individualizing the treatment.

Some modifications will be necessary in order to adapt the array to clinical use. The human STN is substantially larger than its counterpart in the domestic cat, being approximately 10 mm

in length along a dorsolateral axis and 4 mm in width [27]. Approximately the dorsolateral half of the nucleus is dedicated to motor functions [28] and presumably it is this subdivision that the arrays should access in order to ameliorate the symptoms of movement disorders. Thus, the microelectrodes of a clinical device should range in length from approximately 1 to about 6 mm, the longest of these being identical to the longest shafts in the present array. If the array were to be introduced into the human STN approximately along the long axis of the nucleus, via an approach lateral to the caudate nucleus and the 4th ventricle [29] then the array should be at least 4 mm in diameter (or perhaps slightly larger), to allow for a tolerance of at least 1 mm, which appears to be consistent with the best techniques for targeting the existing clinical arrays into the human STN [30]. With the same spacing between electrode shafts as in the present array (350 μm), this array would include about 90 electrodes. While such a device could be fabricated by essentially the same procedure as the present array, it is not certain that the array would need to span the entire width and breadth of the subthalamic nucleus in order to be clinically effective. In the feline nucleus, stimulation at a safe level can modulate the responses of neurons over a distance of approximately 1 mm (Figs. 6, 7). There may be some increased risk of vascular injury during implantation of an array with a footprint that is sufficiently large so as to encompass the entire subthalamic nucleus. Perhaps a prudent strategy for introducing this technology into clinical use would be to proceed in a staged manner using an array of approximately the same diameter as the device described here (or perhaps an array with one extra ring of electrodes, for a total of 32) and modified to ensure that it can provide all of the capabilities of the devices now in clinical use, while also introducing the capabilities for localized microstimulation and for recording of neuronal activity at multiple sites within the nucleus. If these capabilities can be shown to provide increased clinical benefit over the extant devices, then arrays of greater diameter and with additional microelectrodes could be introduced, while carefully monitoring for an increased incidence of vascular damage during implantation.

The array's utility as a clinical and experimental device might be enhanced by replacing some or most of the discrete iridium electrodes with multisite silicon-substrate probes. This would distribute more electrode sites along the array's long axis while also reducing the number of electrode shafts, which may reduce the risk of tissue damage and facilitate fabrication. Especially in a device intended for clinical use, the risks that may arise from the fragility of the silicon-substrate probes must be evaluated carefully.

Any novel array for clinical deep brain stimulation must retain all of the functionality of the devices now in clinical use as well as providing new capabilities. Kuncel and Grill [31] estimated that the extant clinical devices (e.g, Medtronics Soletra) must inject 135–400 nC/ph into the STN in order to elicit the desired clinical effect. These devices have 4 independent macroelectrodes. In order to deliver 400 nC/ph, 4 of our microelectrodes must be configured to have exposed surface areas of approximately 100 000 μm^2, if the charge density is not to exceed 400 $\mu C/cm^2$. This would require removing the insulation from approximately 1 mm of the electrode's tip region. It then will be necessary to investigate the safety issues that are attendant to prolonged stimulating with this combination of charge density and charge per phase, and at the rather high pulse rates (135–185 Hz) that are used for therapeutic deep brain stimulation in the STN.

ACKNOWLEDGMENT

The authors thank C. Graham and J. Chavez for preparation of the histologic material, and assistance with the three-dimensional reconstruction of the electrode sites, D. Minick and A. Tirado for fabrication of the microelectrode arrays, and L. Bullara for assistance with the design of the electrode array. E. Smith provided invaluable assistance with the animal surgeries. They also thank E. Smith and the animal care staff for excellent care of the animals. N. Kuleviciute provide assistance with the long-terms stimulations and C. Long provided secretarial assistance.

The animal studies were approved by the Animal Care & Use Committee of HMRI, and were performed under the guidelines set forth in the Guide to Care and Use of Laboratory Animals (1996 edition)

REFERENCES

[1] K. Ashkan, B. Wallace, B. A. Bell, and A. L. Benabid, "Deep brain stimulation of the subthalamic nucleus in Parkinson's disease 1993–2003: Where are we 10 years on?," *Br. J. Neurosurg.*, vol. 18, pp. 19–34, 2004.

[2] K. E. Lyons and R. Pahwa, "Deep brain stimulation in Parkinson's disease," *Curr. Neurol. Neurosci. Rep.*, vol. 4, pp. 290–295, 2004.

[3] ——, "Deep brain stimulation and essential tremor," *J. Clin. Neurophysiol.*, vol. 21, pp. 2–5, 2004.

[4] E. B. Montgomery Jr., "Deep brain stimulation for hyperkinetic disorders," *Neurosurg. Focus.*, vol. 17, p. E1, 2004.

[5] J. K. Krauss, J. Yianni, T. J. Loher, and T. Z. Aziz, "Deep brain stimulation for dystonia," *J. Clin. Neurophysiol.*, vol. 21, pp. 18–30, 2004.

[6] C. C. McIntyre, M. Savasta, B. L. Walter, and J. L. Vitek, "How does deep brain stimulation work? Present understanding and future questions," *J. Clin. Neurophysiol.*, vol. 21, pp. 40–50, 2004.

[7] C. C. McIntyre and W. M. Grill, "Finite element analysis of the current-density and electric field generated by metal microelectrodes," *Ann. Biomed. Eng.*, vol. 29, pp. 227–235, 2001.

[8] D. B. McCreery, T. G. Yuen, W. F. Agnew, and L. A. Bullara, "Stimulation with chronically implanted microelectrodes in the cochlear nucleus of the cat: Histologic and physiologic effects," *Hear. Res.*, vol. 62, pp. 42–56, 1992.

[9] ——, "Stimulus parameters affecting tissue injury during microstimulation in the cochlear nucleus of the cat," *Hear. Res.*, vol. 77, pp. 105–115, 1994.

[10] D. B. McCreery, T. G. Yuen, and L. A. Bullara, "Chronic microstimulation in the feline ventral cochlear nucleus: Physiologic and histologic effects," *Hear. Res.*, vol. 149, pp. 223–238, 2000.

[11] X. Beebe and T. L. Rose, "Charge injection limits of activated iridium oxide electrodes with 0.2 ms pulses in bicarbonate buffered saline," *IEEE Trans. Biomed. Eng.*, vol. BME-35, no. 6, pp. 494–495, Jun 1988.

[12] L. S. Robblee, J. Lefko, and S. B. Brummer, "Activated Ir: An electrode suitable for reversible charge injection in saline solution," *J. Electrochem. Soc.*, vol. 130, pp. 731–733, 1983.

[13] S. A. Rowland, S. W. Shalaby, R. A. Latour Jr., and A. F. von Recum, "Effectiveness of cleaning surgical implants: Quantitative analysis of contaminant removal," *J. Appl. Biomater.*, vol. 6, pp. 1–7, 1995.

[14] K. V. Romansky, K. G. Usunoff, D. P. Ivanov, and R. Hassler, "Pallidosubthalamic projection in the cat. Electron microscopic study," *Anat. Embryol. (Berl.)*, vol. 159, pp. 163–180, 1980.

[15] I. L'Vovich A, "[Connections between the globus pallidus and putamen and the hypothalamus and subthalamus]," *Arkh. Anat. Gistol. Embriol.*, vol. 74, pp. 35–41, 1978.

[16] S. Afsharpour, "Topographical projections of the cerebral cortex to the subthalamic nucleus," *J. Comp. Neurol.*, vol. 236, pp. 14–28, 1985.

[17] R. M. Beckstead, "A reciprocal axonal connection between the subthalamic nucleus and the neostriatum in the cat," *Brain. Res.*, vol. 275, pp. 137–142, 1983.

[18] A. Abosch, W. D. Hutchison, J. A. Saint-Cyr, J. O. Dostrovsky, and A. M. Lozano, "Movement-related neurons of the subthalamic nucleus in patients with Parkinson disease," *J. Neurosurg.*, vol. 97, pp. 1167–1172, 2002.

[19] S. N. Haber, E. Lynd-Balta, and S. J. Mitchell, "The organization of the descending ventral pallidal projections in the monkey," *J. Comp. Neurol.*, vol. 329, pp. 111–128, 1993.
[20] F. A. Mettler and G. M. Stern, "Somatotopic localization in rhesus subthalamic nucleus," *Arch. Neurol.*, vol. 7, pp. 328–329, 1962.
[21] M. Miyata, "Interconnections between the subthalamic nucleus and the cerebral cortex of the cat," *Neurosci. Res.*, vol. 4, pp. 1–11, 1986.
[22] P. V. Theodosopoulos, W. J. Marks Jr., C. Christine, and P. A. Starr, "Locations of movement-related cells in the human subthalamic nucleus in Parkinson's disease," *Mov. Disord.*, vol. 18, pp. 791–798, 2003.
[23] P. Romanelli, G. Heit, B. C. Hill, A. Kraus, T. Hastie, and H. M. Bronte-Stewart, "Microelectrode recording revealing a somatotopic body map in the subthalamic nucleus in humans with Parkinson disease," *J. Neurosurg.*, vol. 100, pp. 611–618, 2004.
[24] C. C. McIntyre, S. Mori, D. L. Sherman, N. V. Thakor, and J. L. Vitek, "Electric field and stimulating influence generated by deep brain stimulation of the subthalamic nucleus," *Clin. Neurophysiol.*, vol. 115, pp. 589–595, 2004.
[25] P. Pollak, P. Krack, V. Fraix, A. Mendes, E. Moro, S. Chabardes, and A. L. Benabid, "Intraoperative micro- and macrostimulation of the subthalamic nucleus in Parkinson's disease," *Mov. Disord.*, vol. 17, pp. S155–S161, 2002.
[26] D. McCreery, V. Pikov, A. Lossinsky, L. Bullara, and W. Agnew, "Arrays for chronic functional microstimulation of the lumbosacral spinal cord," *IEEE Trans. Neural. Syst. Rehabil. Eng.*, vol. 12, no. 2, pp. 195–207, Jun. 2004.
[27] C. D. Hardman, J. M. Henderson, D. I. Finkelstein, M. K. Horne, G. Paxinos, and G. M. Halliday, "Comparison of the basal ganglia in rats, marmosets, macaques, baboons, and humans: Volume and neuronal number for the output, internal relay, and striatal modulating nuclei," *J. Comp. Neurol.*, vol. 445, pp. 238–255, 2002.
[28] C. Hamani, J. A. Saint-Cyr, J. Fraser, M. Kaplitt, and A. M. Lozano, "The subthalamic nucleus in the context of movement disorders," *Brain*, vol. 127, pp. 4–20, 2004.
[29] A. L. Benabid, A. Koudsie, A. Benazzouz, J. F. Le Bas, and P. Pollak, "Imaging of subthalamic nucleus and ventralis intermedius of the thalamus," *Mov. Disord.*, vol. 17, pp. S123–S129, 2002.
[30] Y. M. Andrade-Souza, J. M. Schwalb, C. Hamani, H. Eltahawy, T. Hoque, J. Saint-Cyr, and A. M. Lozano, "Comparison of three methods of targeting the subthalamic nucleus for chronic stimulation in Parkinson's disease," *Neurosurgery*, vol. 56, pp. 360–368, 2005. discussion 360-8.
[31] A. M. Kuncel and W. M. Grill, "Selection of stimulus parameters for deep brain stimulation," *Clin. Neurophysiol.*, vol. 115, pp. 2431–2441, 2004.

Douglas B. McCreery received the B.Sc. and M.Sc. degrees in electrical engineering and the Ph.D. degree in biomedical engineering from the University of Connecticut, Storrs, in 1966, 1970, and 1975, respectively.

He is currently Director of the Neural Engineering program at Huntington Medical Research Institutes. His research interests include the development of neuroprostheses for the central nervous system, and the physiologic and histologic effects of electrical stimulation of the central and peripheral nervous system.

Dr. McCreery is a member of the Society for Neuroscience.

Albert Lossinsky received the B.A. degree in biology and chemistry from Kansas Wesleyan University, Salina, in 1969, the M.S. degree in microbiology and electron microscopy from Emporia State University, Emporia, KS in 1974, and the Ph.D. degree in neurobiology from the Medical Research Center of the Polish Academy of Sciences, Warsaw, Poland, in 1994.

He is currently the head of the Immunohistochemistry and Scanning Electron Microscopy laboratories within the Neural Engineering Program at Huntington Medical Research Institutes, Pasadena, CA. His research interests include ultrastructural pathology, neurodegenerative changes after electrical stimulation of the brain and spinal cord, and transport across the blood-brain barrier.

Victor Pikov received the B.A. degree in biopsychology from Vassar College, Pougkeepsie, NY, in 1995. In 2000, he received the Ph.D. degree in cell biology at Georgetown University, Washington, DC. He then completed a Boswell postdoctoral fellowship at the California Institute of Technology in 2002.

He is a Research Scientist in the Neural Engineering Program at the Huntington Medical Research Institutes, Pasadena, CA. His research interest is in development of prostheses for the central nervous system.

Xindong Liu received the Ph.D. degree in biomedical engineering in 1995 from Xi'an Jiaotong University, Xi'an, China.

In 1996, he was awarded the James Boswell Postdoctoral Fellowship, cosponsored by the California Institute of Technology, Pasadena, CA and the Huntington Medical Research Institutes (HMRI), Pasadena, CA. He now is a Researcher in the Neural Engineering Program at HMRI. His research interests include biomedical instrumentation, signal processing, computation and modeling, and neuroprostheses.